Structure, Vol. 13, 1559–1568, October, 2005, ©2005 Elsevier Ltd All rights reserved. DOI 10.1016/j.str.2005.07.013

Crystal Structures of the Mnk2 Kinase Domain Reveal an Inhibitory Conformation and a Zinc Binding Site

Ralf Jauch,[1] Stefan Jäkel,[2] Catharina Netter,[3] Kay Schreiter,[2] Babette Aicher,[2] Herbert Jäckle,[1] and Markus C. Wahl[3,*]

[1]Max-Planck-Institut für Biophysikalische Chemie
Abteilung Molekulare Entwicklungsbiologie
Am Faßberg 11
37077 Göttingen
Germany

[2]DeveloGen AG
Marie-Curie-Strasse 7
37097 Göttingen
Germany

[3]Max-Planck-Institut für Biophysikalische Chemie
Abteilung Zelluläre Biochemie/Röntgenkristallographie
Am Faßberg 11
37077 Göttingen
Germany

Summary

Human mitogen-activated protein kinases (MAPK)-interacting kinases 1 and 2 (Mnk1 and Mnk2) target the translational machinery by phosphorylation of the eukaryotic initiation factor 4E (eIF4E). Here, we present the 2.1 Å crystal structure of a nonphosphorylated Mnk2 fragment that encompasses the kinase domain. The results show Mnk-specific features such as a zinc binding motif and an atypical open conformation of the activation segment. In addition, the ATP binding pocket contains an Asp-Phe-Asp (DFD) in place of the canonical magnesium binding Asp-Phe-Gly (DFG) motif. The phenylalanine of this motif sticks into the ATP binding pocket and blocks ATP binding as observed with inhibitor bound and, thus, inactive p38 kinase. Replacement of the DFD by the canonical DFG motif affects the conformation of Mnk2, but not ATP binding and kinase activity. The results suggest that the ATP binding pocket and the activation segment of Mnk2 require conformational switches to provide kinase activity.

Introduction

Control of cellular growth is tightly linked to the regulation of protein synthesis through the eukaryotic initiation factor 4E (eIF4E). eIF4E facilitates the recruitment of mRNA to the translational machinery by binding of the mRNA 5′-cap structure (von der Haar et al., 2004) and is subject to regulation. Nutrition sensing and growth factors regulate formation of productive translation initiation complexes (Richter and Sonenberg, 2005), a process in which eIF4E activity is modulated through phosphorylation by mitogen-activated protein kinases (MAPK)-interacting kinases 1 and 2 (Mnk1 and Mnk2) (Scheper et al., 2001; Waskiewicz et al., 1997, 1999). Both eIF4E and Mnks bind to eIF4G within the initiation complexes. Mnks are activated in turn by MAP kinases such as extracellular signal-regulated protein kinases (ERK) and p38 in response to cytokines, mitogens, or cellular stress (Fukunaga and Hunter, 1997; Scheper et al., 2001; Waskiewicz et al., 1997).

The regulatory effects of Mnk-mediated phosphorylation of eIF4E on translation are still controversial (Knauf et al., 2001; Nikolcheva et al., 2002; Ueda et al., 2004), as are the biological consequences of the lack of Mnk activity in mice and flies. Mice homozygous for a targeted disruption of either one or both Mnk genes show no signs of abnormal development (Ueda et al., 2004), whereas loss of the single *Drosophila* Mnk homolog, Lk6, produces a diet-dependent and eIF4E-mediated growth phenotype (Arquier et al., 2005; Reiling et al., 2005).

Humans possess two *mnk* genes, both of which encode two alternatively spliced transcripts, resulting in the proteins Mnk1a, Mnk1b, Mnk2a, and Mnk2b (Figure 1A; O'Loghlen et al., 2004; Scheper et al., 2003). Sequence alignments reveal a central kinase domain in Mnks, which can be placed into the group of Ca^{2+}/calmodulin-modulated protein kinases (CaMK) (Manning et al., 2002) (Figure 1B) and which is unaffected by alternative splicing (Figure 1A). We have investigated human Mnk2 as a representative of the Mnks, both structurally and functionally. We present the crystal structure of a Mnk2 fragment spanning its kinase domain at 2.1 Å resolution, showing a Mnk-specific zinc binding module and an open conformation of the activation segment (Nolen et al., 2004). In addition, Mnks contain an Asp-Phe-Asp (DFD) motif in place of the otherwise strictly conserved magnesium binding Asp-Phe-Gly (DFG), which exhibits a conformation that obstructs ATP binding. Thus, Mnks are architecturally distinct from other protein kinases. We also present structural and functional data on a Mnk2 mutant containing a canonical DFG motif. Our analysis revealed features relevant for the regulation of activity and inhibition of Mnks and demonstrated that Mnks represent a prototype variation of CaMK group kinases.

Results and Discussion

Organization and Atypical Elements of Mnk2

The central region of Mnks harbors the kinase domain of the proteins (residues 81–368 in human Mnk2; Figures 1A and 1B), according to which Mnks belong to the CaMK group. The N-terminal 80 residues contain a nuclear localization signal (NLS) and a binding motif for eIF4G (Figure 1A). Residues beyond position 368 contribute to the interaction with MAP kinases (Slentz-Kesler et al., 2000) (Figure 1A). Like several other CaMK group members, Mnks are not regulated by Ca^{2+}/calmodulin, in agreement with the lack of a sequence element for the interaction with that protein (Slentz-Kesler et al., 2000).

Protein kinases contain conserved structural elements to bind and activate their protein substrates and the

*Correspondence: mwahl@gwdg.de

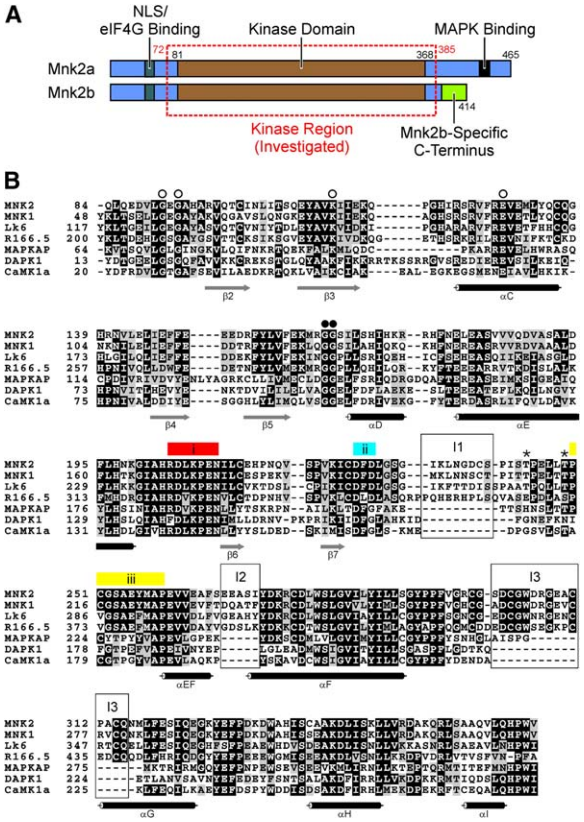

Figure 1. Mnk2 Organization and Sequence Alignment

(A) Schematic comparison of the two splice variants of human Mnk2 indicating the arrangement of functional domains (as labeled). The region investigated herein (Mnk2 kinase region, Mnk2-KR) is boxed. Alternative splicing affects neither the N terminus nor the kinase domain. NLS, nuclear localization signal; eIF4G, eukaryotic initiation factor 4G, the scaffolding protein of the translation initiation complex that binds Mnk1 and Mnk2 (Pyronnet et al., 1999; Scheper et al., 2001).

(B) Sequence alignment of the kinase domains of human Mnk1 and Mnk2, the *Drosophila* and *C. elegans* Mnk orthologs (Lk6 and R166.5, respectively), and three human CaMK group kinases of known structure (MAPKAP, MAP kinase-activated protein kinase). Mnk2 numbering refers to a recently reported sequence (Slentz-Kesler et al., 2000). Secondary structure elements as found in Mnk2-KR are indicated below the alignment. Stars indicate phosphorylation sites (Scheper et al., 2001). The catalytic loop (i), the DFD motif (DFG in other kinases; ii), and the P+1 loop (iii) are marked with colored bars. Insertions characteristic for Mnks are boxed (I1–I3). Open circles mark Gly91 and Gly93 of the glycine-rich loop, Lys113, and Glu129 known to be important for ATP binding (Taylor and Radzio-Andzelm, 1994), filled circles mark Gly164 and Gly165 of the hinge region separating the N-terminal and C-terminal lobes.

cosubstrate ATP (Johnson et al., 1996; Nolen et al., 2004; Taylor and Radzio-Andzelm, 1994). In addition to those, Mnks contain atypical elements such as a DFD motif in place of the canonical magnesium binding DFG motif, and three insertions (I1–I3; Figure 1B), one of which (I3) contains a cluster of four conserved cysteines. We asked whether and how these features affect the structure and function of the kinase domain. While we were able to express and purify the recombinant full-length Mnk2, the protein failed to crystallize. We therefore screened for alternative expression constructs, identifying a truncated version (residues 72–385) that encompasses the kinase domain (Figure 1A) and could be produced in soluble form (see Experimental Procedures). This construct is referred to as the Mnk2-kinase region (Mnk2-KR) herein. Significantly, nonphosphorylated Mnk2-KR is inactive but can be activated by phosphorylation via ERK2 (Figure 2), thus recapitulating the behavior of the full-length protein (Waskiewicz et al., 1997). The nonphosphorylated Mnk2-KR could be crystallized and yielded diffraction data to 2.1 Å resolution (Table 1).

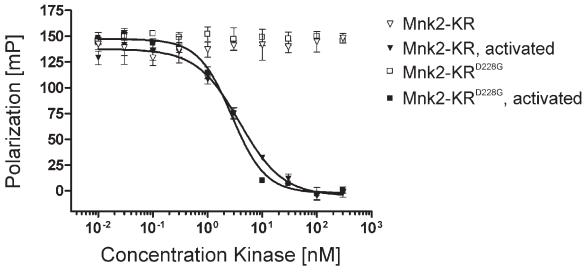

Figure 2. Catalytic Activity of Mnk2-KR and Mnk2-KR^{D228G}

Kinase activity profiles of Mnk2-KR (wild-type and D228G mutant) before and after activation by phosphorylation through ERK2. Kinases were titrated in the indicated concentration range into the Mnk kinase assay (see Experimental Procedures). Data points represent means of triplicates; error bars indicate one standard deviation. The data have been subjected to nonlinear regression analysis by using the four parameter logistic equation (GraphPad Prism software). Results demonstrate that while activation is necessary for both wild-type Mnk2-KR and the D228G mutant, the activated wild-type and mutant kinase domains exhibit almost identical kinase activity (calculated EC_{50}s for Mnk2-KR and Mnk2-KR^{D228G} are 3.8 and 2.8 nM, respectively).

Structure Solution and Architecture of the Mnk2 Kinase Region

The structure of Mnk2-KR was solved by molecular replacement by using as a search model the structure of the death-associated protein kinase 1 (DAPK1; PDB ID 1JKS; Tereshko et al., 2001), another CaMK group member that exhibits about 30% amino acid identity with Mnk2-KR. The final Mnk2-KR model and the DAPK1 structure compare with an average rmsd of 1.32 Å over 211 matching Cα atoms. The Mnk2-KR crystal structure was refined to a final R/R_{free} value of 21.5%/25.4% and maintained good overall geometry (Table 1). A total of 16 residues at the C terminus of Mnk2-KR, which do not pertain to the core kinase domain (Figure 1A), as well as residues 232–250 (part of the activation segment) and 306–309 (part of insertion I3), which are situated in flexible regions, did not show up in the final $2F_o$-F_c electron density and have been omitted from the model.

Mnk2-KR displays the typical bilobal arrangement of a protein kinase, with the ATP binding cleft sandwiched between an N-terminal and a C-terminal lobe (Figure 3A). The N-terminal lobe contains a twisted β sheet (β2–β5; numbering of secondary structure elements is ac-

Table 1. Crystallographic Data

	Mnk2-KR Wild-Type	Mnk2-KR^{D228G}
Data Collection		
Wavelength (Å)	1.05	1.05
Space group	$P3_221$	$P3_221$
Cell dimensions (Å)		
a (= b)	104.5	104.6
c	72.3	73.4
Resolution (Å)	30.0–2.1 (2.2–2.1)[a]	30–3.2 (3.3–3.2)
R_{sym}[b] (%)	5.2 (37.3)	4.1 (46.2)
I/σI	31.6 (3.4)	14.5 (1.8)
Completeness (%)	99.5 (99.9)	98.2 (99.0)
Refinement		
Resolution (Å)	15.0–2.1	30–3.2
Number of reflections	24,664	7,768
R_{work}/R_{free}[c] (%)	21.5/25.4	23.8/30.6
Number of atoms		
Protein	2,217	2,205
Zn^{2+}	1	1
Water	161	18
B factors		
Protein	75.8	75.6
Water	77.4	53.1
Wilson	60.1	68.5
Rms deviations from ideal		
Bond lengths (Å)	0.009	0.009
Bond angles (°)	1.21	1.56

[a] Values for the highest 0.1 Å resolution shell in parentheses.
[b] $R_{sym}(I) = (\Sigma_{hkl}\Sigma_i[|I_i(hkl) - <I(hkl)>|]/\Sigma_{hkl}\Sigma_i[I_i(hkl)]$; $I_i(hkl)$, intensity of the i^{th} measurement of hkl; $<I(hkl)>$, average value of hkl for all i measurements.
[c] $R_{work} = \Sigma_{hkl}[||F_{obs}| - k|F_{calc}||]/\Sigma_{hkl}[|F_{obs}|]$; $R_{free} = \Sigma_{hkl \subset T}[||F_{obs}| - k|F_{calc}||]/\Sigma_{hkl \subset T}[|F_{obs}|]$; $hkl \subset T$, test set.

cording to the standard nomenclature of kinase topology; Knighton et al., 1991a) and an α helix (αC). While the N-terminal part of the protein runs in antiparallel fashion along the edge of strand β2, it does not engage in continuous β-type backbone pairing to the β sheet; therefore, the present structure of Mnk2-KR formally lacks strand β1 (Figures 1B and 3A). The conserved residue Glu129 of helix αC participates in an ionic interaction with Lys113 in β3, as required for stabilizing the ATP substrate (Taylor and Radzio-Andzelm, 1994). The glycine-rich loop (residues 90–94) is flexible and contains the conserved residues Gly91 and Gly93, which play key roles in ATP binding (Taylor and Radzio-Andzelm, 1994). The C-terminal lobe (residues 166–368) starts downstream of the "hinge" connector region (Gly164, Gly165) and contains a predominantly hydrophobic four-helix bundle (αD–αF, αH). Arg204 (which defines the RD kinases that are often activated by phosphorylation [Johnson et al., 1996]), Asp205 (the catalytic aspartate), and Asn210 (which serves in active kinases to coordinate a catalytic magnesium ion [Adams, 2001]) are situated in the catalytic loop (C loop, residues 204–210). In addition, the C-terminal lobe harbors the activation segment (residues 226–260; Nolen et al., 2004; Figure 3A), which is required for binding the protein substrate.

Inhibitory Conformation of the Activation Segment

The magnesium binding loop (residues surrounding the DFD motif), the activation loop (disordered residues preceding the P+1 loop), and the P+1 loop (residues 250–259) constitute the activation segment (Figure 3A; Nolen et al., 2004). It is followed C-terminally by the short helix αEF (residues 260–265) and the long helix αF (residues 270–290), the latter being part of the four-helix bundle in the C-terminal lobe (Figure 3A). The P+1 loop was shown to interact with a residue adjacent to the phosphorylation site (Knighton et al., 1991b). Together with the adjoining helix αEF, the P+1 loop represents subdomain VIII (Hanks and Quinn, 1991), which in active protein kinases is cradled in a predominantly hydrophobic environment provided by αF, αG, and the C loop. In the present Mnk2-KR crystal structure, helix αF is N-terminally extended due to a Mnk-specific insertion (I2; Figure 1B). As a consequence, the protein disengages the canonical intramolecular interaction between subdomain VIII and the αF/αG/C loop region, and, instead, two symmetry-related, neighboring molecules in the crystal reciprocally insert their activation segments into the C-terminal lobe of the symmetry mate (Figure 3B). This intermolecular interaction observed for Mnk2-KR maintains conserved polar interactions between subdomain VIII and the αF/αG/C loop region, which are normally built up intramolecularly (as seen, e.g., in DAPK1; Figure 3C, Figure S1; see the Supplemental Data available with this article online), including a hydrogen bond between Ser253 (P+1 loop) and Asp205 (C loop) as well as a Glu260-Arg356 ion pair (Figure 3C).

Because protein kinases require the interaction of the P+1 loop with the C loop for substrate binding and since such an interaction is fostered intermolecularly in

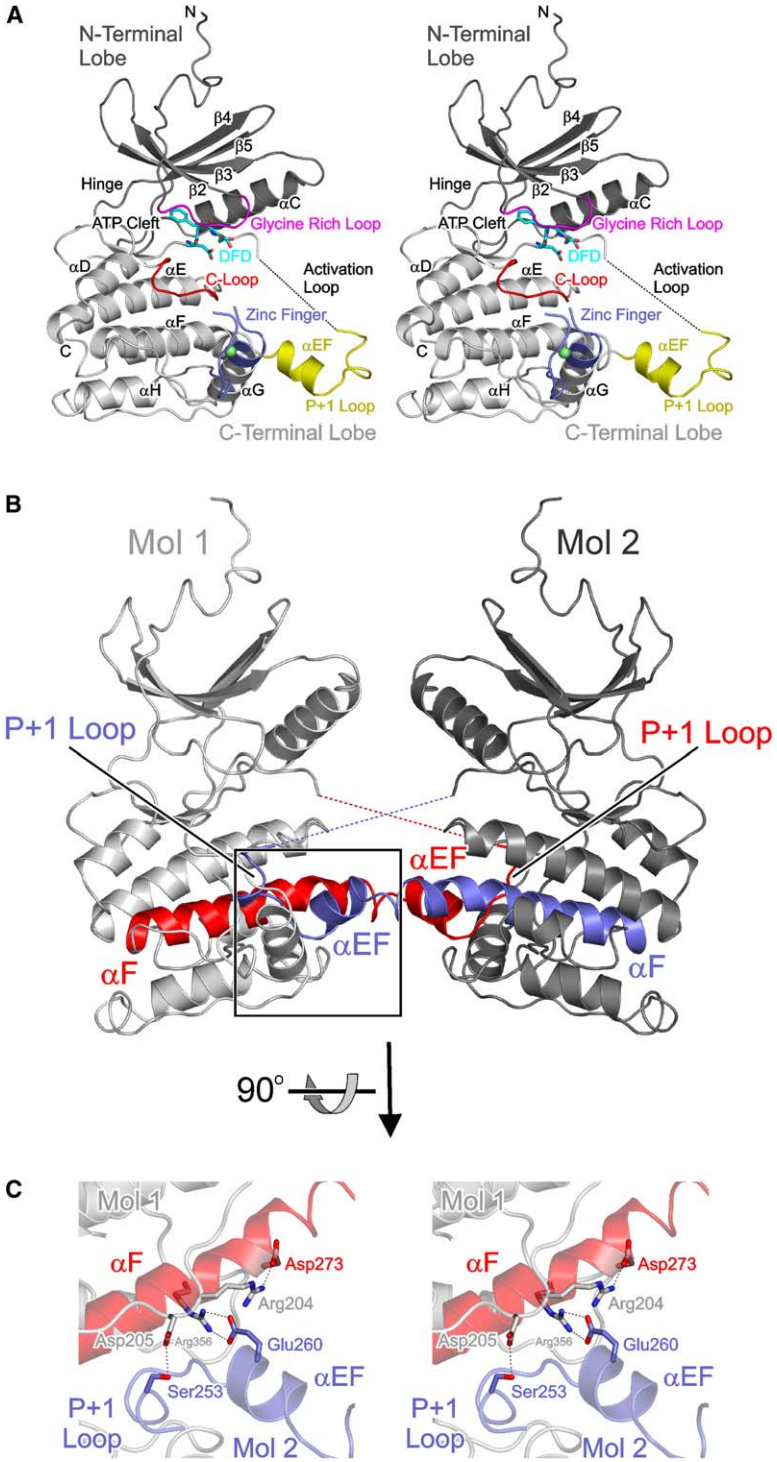

Figure 3. Overall Structure of Mnk2-KR and the Extruded Activation Segment

(A) Stereo ribbon plot displaying the overall Mnk2-KR structure. Prominent structural elements are displayed in colors and labeled according to standard nomenclature (Knighton et al., 1991a). The magnesium binding loop (around the DFD motif), the activation loop, and the P+1 loop constitute the activation segment. Subdomain VIII is in yellow (Hanks and Quinn, 1991). Note that the glycine-rich loop (pink) exhibits partially disordered side chains and that residues Gly232–Cys251 are missing in the final electron density (dotted line). The missing portion encompasses part of the activation loop, including Thr244 and Thr249, which are phosphorylated by upstream activating kinases. Another region with partially missing electron density and high temperature factors corresponds to the insertion with the specific cysteine cluster (residues 304–310; tip of the zinc finger). Green sphere: zinc ion.

(B) Side view of two neighboring Mnk2-KR molecules in the crystal lattice (Mol1 and Mol2, light and dark gray, respectively), which show a reciprocal interaction via the P+1 loop and helix αEF (red for Mol1, blue for Mol2). The left molecule (Mol1) is rotated 20° clockwise about the vertical axis compared to the view in (A).

(C) Stereo ribbon plot showing details of the interaction of the αEF/P+1 loop portion of one molecule (Mol 2, blue) with the C-terminal lobe of a neighboring molecule in the crystal (Mol1, gray, with αF in red). Residues involved in the conserved polar interaction are highlighted as sticks. Atoms are color coded by atom type (carbon, as the respective protein backbones; oxygen, red; nitrogen, blue). The view is on the boxed region in (B) rotated 90° about the horizontal axis as indicated.

the present crystal structure, the arrangement of two Mnk2-KR molecules within the crystals suggested a functionally relevant dimer formation. However, multi-angle laser light scattering and analytical gel filtration chromatography showed that Mnk2-KR is a monomer in solution (data not shown). Therefore, the interaction of the P+1 loop and the C loop, as required for substrate binding, is not promoted by intermolecular contacts in solution. An extruded activation segment, as observed in the present structure, could therefore be one reason why nonphosphorylated Mnk2 and Mnk2-KR are inactive (Figure 2). Upon phosphorylation, the proteins acquire kinase activity (Figure 2), consistent with the notion that after phosphorylation the activation segment of Mnk2 flips inward so that it can establish the necessary intramolecular contacts with the αF/αG/

C loop region. Significantly, in the present inactive conformation, Arg204 from the C loop forms a salt bridge with Asp273 in helix αF (Figure 3C) that immediately follows the Mnk-specific insertion I2 (Figure 1B). Thus, by positioning Asp273, Arg204 stabilizes the extruded conformation of the activation segment in inactive Mnk2-KR. As known from other RD kinases (Johnson et al., 1996), Arg204 engages in contacts with a phosphate group after activation. The engagement of Arg204 in an alternative interaction with a phosphate after phosphorylation would release Asp273, which in turn could allow for the structural rearrangement of the activation segment required for activity.

Inhibitory Conformation of the Magnesium Binding Loop

Protein kinases contain a conserved DFG motif (residues 226–228; Figure 3A). The first aspartate of this motif is known to coordinate a Mg^{2+} ion, which is needed to activate the γ-phosphate of ATP through polarization (Taylor and Radzio-Andzelm, 1994). The Mnk2-KR contains a DFD motif (residues 226–228) in place of the canonical DFG motif normally found in protein kinases. This DFD fingerprint is unique within the human kinome, but is conserved within the Mnk subfamily (Figure 1B). As compared to the DFG motif of, for example, DAPK1, the DFD motif of the Mnk2-KR is rotated by almost 180° (Figures 4 and 5A). As a result, Phe227 is displaced from its standard position in active kinases and sticks into the ATP binding pocket (Figure 4A), thus excluding ATP from its binding site. The residue also blocks an access route for the nucleotide to the pocket (Figure 4B). Thus, the arrangement of the DFD motif in Mnk2-KR interferes with the generic mode of ATP binding (Figure 4C).

The present conformation of the DFD motif is stabilized by (i) a hydrogen bonding interaction of the carbonyl oxygen of Phe227 with the side chain amino group of Lys113, and by (ii) positioning of the Phe227 side chain in a hydrophobic pocket formed primarily by Leu143 and the nonconserved Phe159 (which corresponds to the so-called gatekeeper residue that acts as a selectivity filter for ATP-competitive drugs (Cohen et al., 2005; Figure 4A). The Mnk-specific Asp228 does not participate in stabilizing this conformation by direct interactions.

The noncanonical arrangement of the DFD motif in Mnk2-KR is referred to as the "DFG/D-OUT" conformation, as opposed to the standard "DFG/D-IN" conformation found, e.g., in DAPK1 (Tereshko et al., 2001). A DFG/D-OUT conformation in the Mg^{2+} binding loop was initially found in the apo form of the insulin receptor kinase (IRK), a tyrosine kinase (TK) (Hubbard et al., 1994). A similar DFG/D-OUT conformation is observed in cocrystals of tyrosine kinases such as the cellular protein encoded by Abelson gene (c-Abl), cKIT as well as the vascular endothelial growth factor receptor (VEGF-R) kinase with their inhibitors Gleevec and AAL-993, respectively (Nagar et al., 2002). It is also found in the Ser/Thr kinase p38 when bound to diaryl urea scaffold molecules (Figure 4D; Pargellis et al., 2002). The latter substances, termed "allosteric inhibitors," switch the DFG/D-IN conformation found in the inhibitor-free p38 (Wilson et al., 1996) into a DFG/D-OUT conformation, in which the central phenylalanine blocks ATP binding by sterical hindrance, as observed with Mnk2-KR.

Since the DFG/D-OUT conformation would prevent productive ATP binding (Figure 4C), a switch of DFG/D-OUT into DFG/D-IN is a prerequisite for ATP binding in Mnk2-KR. The proposed structural rearrangement can be modeled without sterical clashes (Figure 4A).

Replacement of DFD by the Canonical DFG Motif

As described, we did not observe any direct interactions of the Mnk-specific Asp228 of the DFD motif with other protein residues, and this finding led us to question its importance for the DFG/D-OUT conformation. To clarify this point, we replaced Asp228 with a glycine and solved the corresponding Mnk2-KR^{D228G} structure at 3.2 Å resolution. The Fo-Fc "omit" electron density map of the DFG region suggests that the Mnk2-KR^{D228G} molecules in the crystals adopt both the DFG/D-IN and the DFG/D-OUT conformations (Figure 5B). Therefore, the replacement of the DFD motif in Mnks by the generic DFG motif destabilizes DFG/D-OUT in favor of DFG/D-IN. The alternative conformation observed in the Mnk2-KR^{D228G} mutant also shows that there are indeed no structural constrains that would prevent the switch of the DFD motif into DFG/D-IN (Figure 4A).

Together, the above observations suggest that Asp228 moderately stabilizes DFG/D-OUT, although it is not involved in direct intramolecular interactions in the present crystal structure. When modeling a DFD/G-IN conformation of a DFD motif based on the structure of the Mnk2-KR^{D228G} mutant (Figure 4A), no direct interactions involving Asp228 can be discerned either. The overall exposure of Asp228 to the aqueous environment in either conformation seems to be similar as well (Figure 4B). In addition, we cannot discern decisive differences in the electrostatic potentials around the DFD motif that would favor the DFG/D-OUT or -IN conformations (Figure 4B). One possibility is that interactions involving Asp228 ensue in a slightly modified conformation in solution and that the DFG/D-OUT conformation has been trapped in the crystals. Gly228 in place of Asp228 in the Mnk2-KR^{D228G} mutant may foster increased backbone flexibility, which could then allow the protein to adopt both conformations.

We next asked whether the DFG/D-OUT to DFG/D-IN switch that is necessary for ATP binding requires factors other than ATP itself. ATP binding assays with nonphosphorylated Mnk2-KR, with phosphorylated and thereby activated Mnk2-KR, and with Mnk2-KR^{D228G} showed that both Mnk2-KR and Mnk2-KR^{D228G} were able to bind ATP and that binding occurred irrespective of the phosphorylation-dependent activation of the proteins (Figure 5C). However, only the phosphorylated forms of Mnk2-KR and Mnk2-KR^{D228G} exerted kinase activity (Figure 2). These results establish that phosphorylation of Mnk2-KR is a prerequisite for catalytic activity, but not for ATP binding, and that neither aspect depends on Asp228 of the DFD motif.

Since our solution studies showed that ATP is able to bind to nonphosphorylated Mnk2-KR (Figure 5C), we attempted to cocrystallize the protein with ATP, ATP/

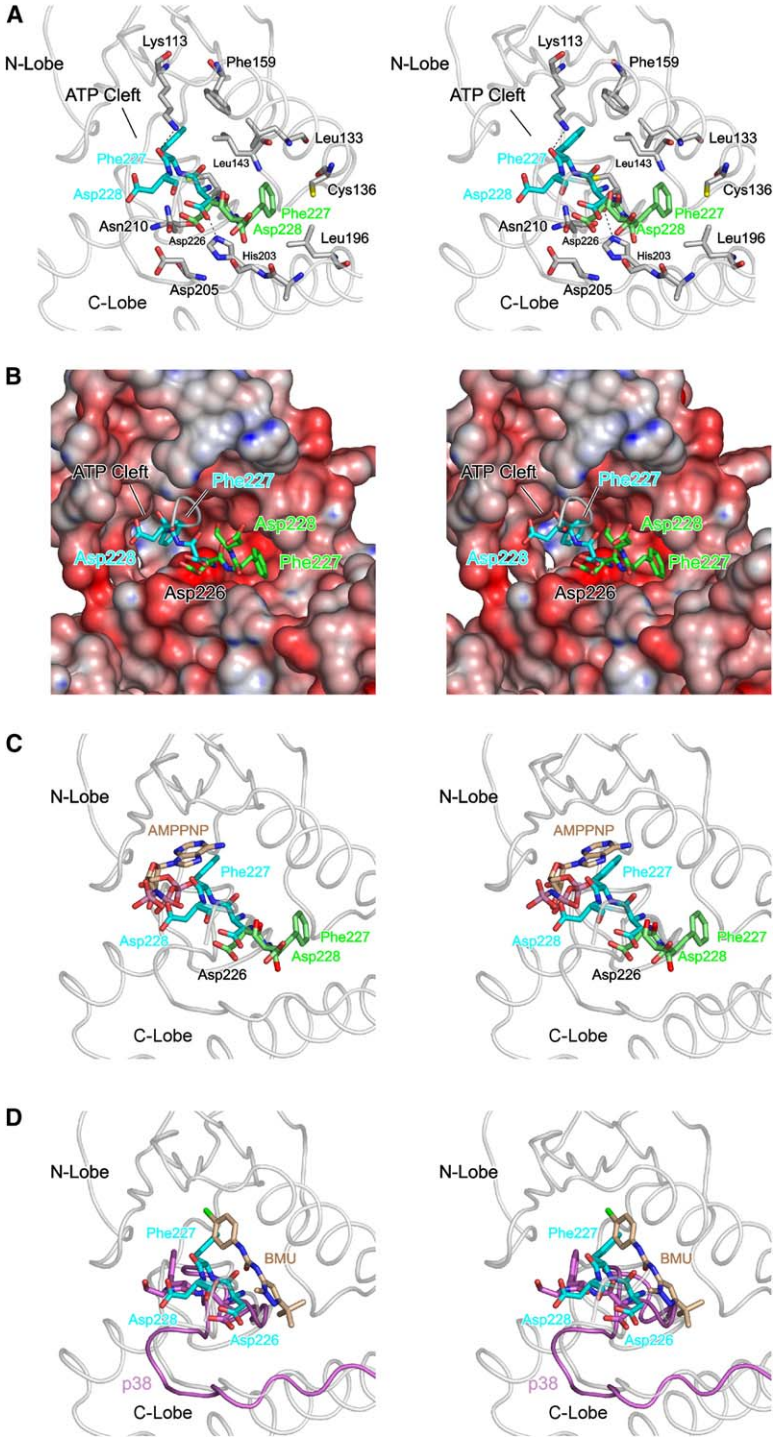

Figure 4. Neighborhood of the DFD Motif

(A) Close-up stereoview of the DFD region and the ATP binding cleft. The DFG/D-OUT conformation of wild-type Mnk2-KR is indicated by a stick representation for Asp226, Phe227, and Asp228 on the upper left with Phe227 and Asp228 poking into the ATP binding cleft (carbon, cyan). A DFG/D-IN conformation (lower right; carbon, green) has been modeled according to the DFG/D-IN conformation seen in other kinases and as observed for the Asp228Gly mutant of Mnk2-KR (see Figure 5B). A backbone trace of Mnk2-KR is shown as a semitransparent gray tube. Residues within a radius of 4 Å around the DFD motif in either the DFG/D-IN or -OUT conformations are displayed as sticks (carbon, gray). Direct interactions with the protein matrix, which stabilize the DFG/D-OUT conformation, are indicated by dashed lines. Phe227 comes to lie in two different hydrophobic pockets in the two different conformations. No obstacle for adoption of a DFG/D-IN conformation is visible. Relative to Figure 3A, the molecule has been rotated 90° clockwise about the vertical axis.

(B) Stereoview of the molecular surface of Mnk2-KR color coded by electrostatic potential (blue, positive charge; red, negative charge), with the two conformations of the DFD motif as a stick representation (color coding as in [A]). The ATP binding cleft is pointed out. Asp228 in either conformation is well accessible to the aqueous solvent. The DFG/D-OUT conformation not only positions Phe227 and Asp228 in the ATP binding cleft, but also obstructs access to this cleft from the front. The molecule has been rotated by 30° about the horizontal axis (N-terminal lobe to back) relative to (A) in order to afford an unobstructed view into the DFD pockets.

(C) Same view as in (A) with a nonhydrolyzable ATP analog (adenosine 5′-[β,γ-imido]-triphosphate [AMPPNP]); carbon, beige; phosphorus, violet) superimposed as seen in the cocrystal structure with DAPK1 (PDB ID 1IG1). In the DFG/D-OUT conformation, the adenine base clashes with the side chain of Phe227, and the phosphate groups clash with the side chain of Asp228.

(D) The same view as in (A) and (C) with only the DFG/D-OUT conformation shown. The DFG region of a p38-BMU inhibitor complex (PDB ID 1KV1) is shown for comparison (magenta tube; DFG in stick representation; carbon, magenta) as seen after global superpositioning of the protein structures. The BMU inhibitor (carbon, beige; chloride, green) occupies part of the DFG/D-IN binding pocket and induces a DFG/D-OUT conformation in p38.

Mg^{2+}, or the nonhydrolyzeable analog AMPPNP with and without Mg^{2+} or to soak preformed crystals with these substances in order to directly visualize conformational changes taking place upon nucleotide binding. Despite extensive efforts, we were not able to obtain crystals of the ATP bound form. Indirectly, these negative results suggest that indeed conformational changes take place upon ATP binding.

A Zinc Binding Motif in Mnk2

Among the Mnk-specific insertions, a region containing four conserved cysteine residues stands out (I3; Figure 1B). In the present crystal structure, the four cysteines are arranged in a manner suggesting a metal ion binding site (Figure 6A). In order to verify the presence of a metal ion in the protein, we recorded the X-ray fluorescence spectrum of frozen Mnk2-KR crystals. Kα and

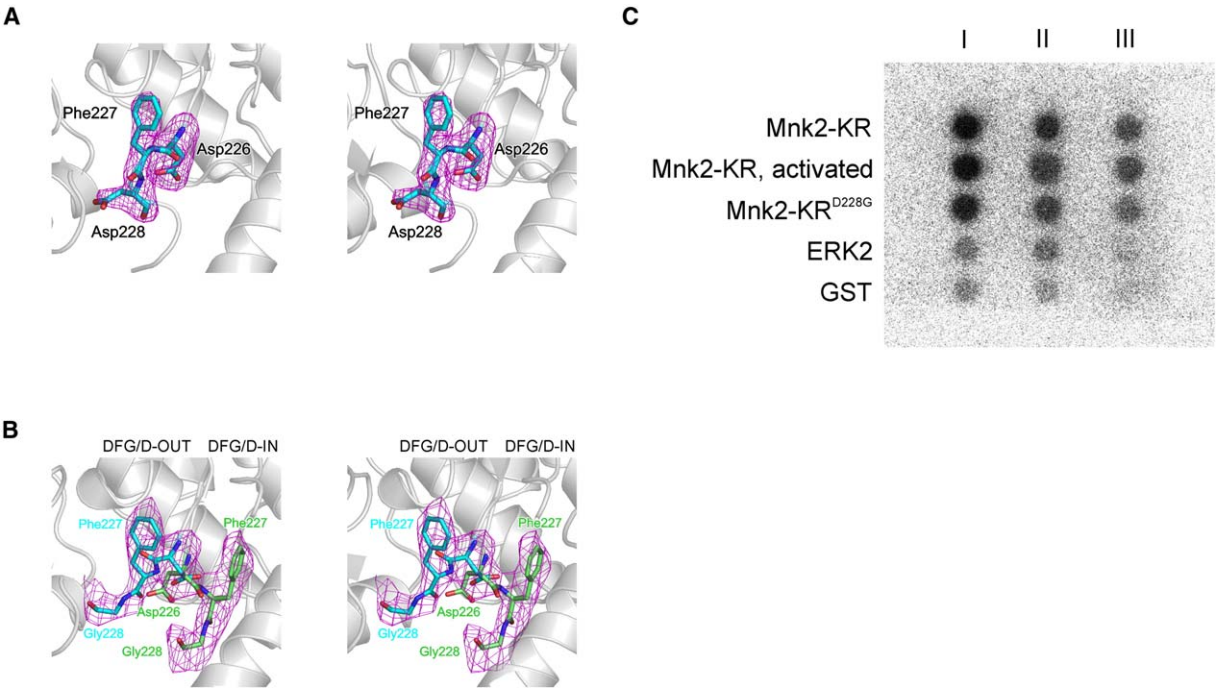

Figure 5. Conformation of the DFD Motif and ATP Binding

(A) Stereo plot showing the Fo-Fc "omit" electron density contoured at the 3σ level covering the DFD motif (sticks; carbon, cyan) in wild-type Mnk2-KR (gray ribbon). Relative to Figure 3A, the molecule has been rotated 90° clockwise about the vertical axis and 90° about the horizontal axis (N-terminal lobe to front), affording a view from the N-terminal lobe onto the motif. Only the DFG/D-OUT conformation is visible in wild-type Mnk2-KR.

(B) Stereo plot showing the Fo-Fc "omit" electron density contoured at the 2.5σ level covering the DFG motif in Mnk2-KR^{D228G}. The DFG motif is found in both a DFD/G-IN (carbon green) and in a DFD/G-OUT (carbon, cyan) conformation in the mutant.

(C) Dot blot assaying the binding of α^{32}-ATP to the indicated proteins at concentrations of 2.8 μM (I), 1.4 μM (II), and 0.7 μM (III). GST, negative control using glutathione S-transferase.

Kβ emission lines characteristic of a zinc ion were observed (Figure 6B). Significantly, Zn^{2+} was never added during the expression, purification, or crystallization of the protein and, therefore, must have been scavenged spontaneously by the protein from the cellular environment. To locate the zinc ion within the Mnk2-KR structure, we reprocessed the original Mnk2-KR diffraction data and kept the Friedel pairs separated. While the diffraction data were collected at a wavelength of 1.05 Å, i.e., remote from the Zn K edge (about 1.28 Å), the anomalous signal expected at that wavelength (~2.7e) is still strong compared to the maximum signal around the edge (~3.9e). Indeed, the Fourier map calculated from the model phases and the anomalous intensity differences revealed a single peak at ~6σ above the background, which maps to the center of the four cysteine SH groups (Figure 6A). Therefore, we conclude that Mnk2 bears a zinc finger-like module within the kinase domain.

We do not expect a direct effect of the zinc finger on the catalytic activity since it is positioned far away from the catalytic center. In zinc fingers of other proteins, zinc ions contribute to the shaping and compaction of short structural motifs, which often provide a binding platform for proteins and/or nucleic acids (Krishna et al., 2003). Thus, we assume that the Mnk-specific zinc finger serves as a docking site for phosphorylation targets and/or regulators. Studies to test the significance of the Mnk-specific zinc finger in vivo are in progress.

Conclusions

Herein, we have investigated a truncated form of human Mnk2 (Mnk2-KR) that covers the kinase domain and exhibits phosphorylation-dependent activity indistinguishable from that of the full-length protein. Our results provide evidence that Mnks represent a distinct protein kinase subfamily. This subfamily is characterized by three insertions that lead to an open conformation of the activation segment in the nonphosphorylated Mnk2-KR and a zinc-coordinating cysteine cluster. Adoption of the active conformation of the activation segment after phosphorylation may be triggered by a phosphate-mediated disruption of an Arg204-Asp273 salt bridge that otherwise stabilizes the inactive, extruded conformation of the activation segment. In addition, we observed a DFD motif that favors an inhibitory DFG/D-OUT conformation in contrast to other unliganded Ser/Thr kinases. Interestingly, the DFG/D-OUT conformation has no qualitative effect either on the ATP binding properties of nonphosphorylated Mnk2-KR or on the catalytic activity after phosphorylation, suggesting that it is marginally stable in the present structure.

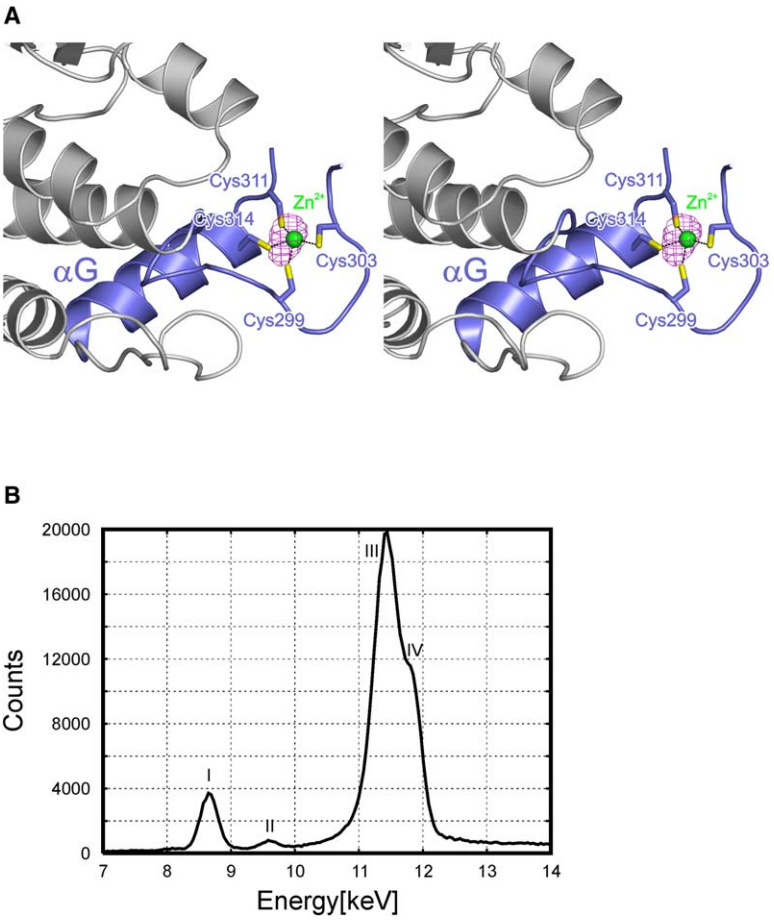

Figure 6. Zinc Binding Site

(A) Stereo ribbon plot of the zinc finger motif in Mnk2-KR (blue). The cluster of four cysteines is indicated by sticks at the tip of the finger (carbon, blue; sulfur, yellow). They surround a zinc ion (green sphere). A Fourier map using the anomalous intensity differences and phases from the refined model is shown contoured at the 5σ level and identifies the position of the anomalous scatterer. The region from Trp305 to Glu309 lacks unambiguous backbone density and has been omitted from the model. The molecule has been rotated 90° counterclockwise about the vertical axis compared to Figure 3A.

(B) X-ray emission spectrum of native Mnk2-KR crystals irradiated with X-rays of λ = 1.05 Å. Peaks in the spectrum correspond to I = Zn-Kα line, II = Zn-Kβ line, III = Compton scattering, IV = elastic scattering.

The latter notion is in agreement with the lack of direct interactions of the Mnk-specific Asp228 that would fasten the DFG/D-OUT conformation. Since both, ATP binding and kinase activity, require an open ATP binding pocket, the switch into the DFG/D-IN conformation might be imposed by ATP binding per se, again consistent with a weak intramolecular stabilization of the DFG/D-OUT conformation in the Mnk2-KR structure. The question remains of whether a regulatory potential via interconversion of DFG/D-IN and -OUT conformations could be realized in vivo, e.g., by interaction with other regulatory proteins or by the protein adopting other conformations in solution.

Since the DFG/D-OUT conformation of Mnk2 is rarely observed in inhibitor-free protein kinases, it provides a handle for specific inhibitor design that would extend the range of generic ATP-competitive compounds (Mol et al., 2004), a speculation that is supported by the binding of the DFG/D-OUT-inducing p38 inhibitor BIRB-796 to Mnk2 (Fabian et al., 2005). Also, the Mnk-specific Asp228 may aid inhibitor design because it renders the Mg^{2+} binding loop unique among Ser/Thr kinases.

Experimental Procedures

Cloning

A cDNA fragment of human Mnk2 (amino acid residues 72–385; Entrez AAG26336), which encompasses the kinase domain, was amplified with the forward/reverse primer pair 5′-CGGGATCCACC GACAGCTTCTCGGGCAGG-3′/5′-ACGCGTCGACACTACCTCTGC AGGACCATGGGAG-3′ (restriction sites are underlined) and was cloned into the BamHI and SalI sites of the vector pGEX-4T1 (Amersham, Uppsala, Sweden). The amino acid substitution Asp228Gly was introduced into the GST-Mnk2-KR construct by employing the Stratagene (Heidelberg, Germany) Quik Change Site Directed Mutagenesis kit according to the manufacturer's instructions. Mutagenesis oligonucleotides were 5′-GAAGATCTGTGACTTCGGCCT GGGCAGCGGCATCAAACTC-3′ and 5′-GAGTTTGATGCCGCTGC CCAGGCCGAAGTCACAGATCTTC-3′.

Protein Preparation

Expression of GST-Mnk2-KR or GST-Mnk2-KR^{D228G} was performed in *E. coli* BL21. Cells were grown in LB medium (Merck, Darmstadt, Germany) supplemented with ampicillin (100 μg/ml; 37°C). Expression was induced at an OD_{600} of 0.8 with 1 mM isopropyl thiogalactoside (4 hr; 25°C). Cells were harvested by centrifugation and resuspended in 10 ml lysis buffer (50 mM Tris/HCl [pH 7.5], 200 mM NaCl, 5 mM DTT) per gram wet weight. Lysates were prepared by sonication and subsequent clearing in a Sorvall SS34 rotor (18,000 rpm, 45 min, 4°C). The supernatant was applied to two GSTPrep FF 16/10 columns (Amersham) connected in series and equilibrated with lysis buffer.

Wild-type or mutated Mnk2-KR were eluted by on-column thrombin cleavage from the GST tag. A total of 1000 units of thrombin (Amersham) was dissolved in 60 ml wash buffer and cycled over the columns (overnight, 8°C). After collection, the thrombin eluate was diluted (1:5 in 50 mM Tris/HCl [pH 8.0]), applied to a 25 ml Q sepharose HP column (Amersham), and eluted with a linear gradient of sodium chloride (50 mM Tris/HCl [pH 8.0], 0–1 M NaCl). Frac-

tions were pooled, concentrated (~16 mg/ml), and transferred into 10 mM Tris/HCl (pH 7.5), 50 mM NaCl, 1 mM DTT via a PD10 column (Amersham). Typically, the final protein concentration was approximately 12 mg/ml.

Crystallographic Analysis

Crystals of wild-type Mnk2-KR and of Mnk2-KR^{D228G} were grown by vapor diffusion with a reservoir solution containing 23% (w/v) polyacrylic acid 5100, 2% (v/v) 2-methyl-2,4-pentane-diol, and 0.1 M HEPES/NaOH (pH 7.7) and were frozen (liquid nitrogen) in reservoir solution supplemented with 12.5% glycerol and 12.5% ethyleneglycol. Diffraction data (Table 1) were collected on beamline BW6 (DESY, Hamburg, Germany) at 100 K on a MarResearch (Norderstedt, Germany) CCD detector and were processed with the HKL package (Otwinowski and Minor, 1997).

The Mnk2-KR structure was solved by molecular replacement (MolRep; [CCP4, 1994]) by using the structure coordinates of DAPK1 (PDB ID 1JKS) as the search model. Model building was conducted automatically by using arp/warp (Cohen et al., 2004) and manually by using Xfit (McRee, 1999). Refinement was performed with CNS (Brunger et al., 1998) and Refmac5 (CCP4, 1994) by using standard protocols. All data between 15.0 and 2.1 Å resolution were employed in the refinement; 5% of the reflections were set aside to monitor R_{free} (Table 1). In the last refinement cycles, different overall anisotropic temperature factor corrections were applied to the N-terminal lobe and the C-terminal lobe by using the TLS refinement option of Refmac5. The structure of Mnk2-KR^{D228G} was subsequently solved by molecular replacement by using the refined Mnk2-KR structure and was refined with CNS.

Gel Filtration and Light Scattering

Gel filtration chromatography was carried out with a SMART system by using a Superdex 75 PC 3.2/30 column (Amersham). Experiments were performed at room temperature in 20 mM Tris/HCl (pH 7.5), 100 mM NaCl, 1 mM DTT at a flow rate of 0.04 ml/min. The molecular weight of Mnk2-KR was estimated by using standard proteins (BioRad, Munich, Germany). Multiangle laser light scattering with a 30 μM solution of Mnk2-KR in the same buffer was performed as described elsewhere (Jauch et al., 2003).

Kinase and Dot Blot Assays

Mnk2, Mnk2-KR, and Mnk2-KR^{D228G} (2.5 μM) were activated with 140 nM preactivated ERK2 and 50 μM ATP in 20 mM HEPES/KOH (pH 7.4), 10 mM $MgCl_2$, 0.25 mM DTT, and 0.05% (w/v) polyoxyethylene 20 stearylether (Brij 78; Sigma, Munich, Germany) for 45 min at 30°C. In vitro kinase activity was assayed in the presence of 30 μM eIF4E-derived substrate peptide and 20 μM ATP in a buffer of 20 mM HEPES/KOH (pH 7.4), 10 mM $MgCl_2$, 0.5 mM DTT, 0.1% (w/v) bovine serum albumin, and 0.01% (w/v) Pluronic F127 (Sigma). Reactions (40 min, 30°C) were terminated by EDTA addition. Substrate phosphorylation was detected based on a competitive fluorescence polarization format (Seethala and Menzel, 1998).

For the dot blots, 0.7–5 μM protein was incubated with a 10 μM mixture of ATP and α^{32}P-ATP (0.2 μCi; Hartmann Analytic, Braunschweig, Germany) in 10 mM Tris/HCl (pH 7.5), 100 mM NaCl, 10 mM $MgCl_2$ (30–60 min at room temperature). Proteins were transferred onto nitrocellulose membranes by using the Minifold I vacuum filtration system (Schleicher & Schüll, Dassell, Germany), washed, and detected by autoradiography.

Supplemental Data

Supplemental Data including a figure showing how one Mnk-2KR molecule inserts its activation segment into the C-terminal lobe of a neighboring molecule in the crystal and a comparison of the conformation of the Mnk-2KR activation segment to that of DAPK1 and MAPKAP2 are available at http://www.structure.org/cgi/content/full/13/10/1559/DC1/.

Acknowledgments

We thank Monique Erling for excellent technical support in protein production and purification and Gleb Bourenkov (Deutsches Elektronensynchrotron, Hamburg) for help with diffraction studies. This work was in part supported by the Max-Planck Gesellschaft (H.J. and M.C.W.). C.N. is a fellow of the Boehringer Ingelheim Fonds. This work is part of the scientific research conducted in the International PhD Program Molecular Biology-International Max Planck Research School at the Georg August University, Göttingen, Germany.

Received: May 30, 2005
Revised: July 18, 2005
Accepted: July 19, 2005
Published: October 11, 2005

References

Adams, J.A. (2001). Kinetic and catalytic mechanisms of protein kinases. Chem. Rev. *101*, 2271–2290.

Arquier, N., Bourouis, M., Colombani, J., and Leopold, P. (2005). *Drosophila* Lk6 kinase controls phosphorylation of eukaryotic translation initiation factor 4E and promotes normal growth and development. Curr. Biol. *15*, 19–23.

Brunger, A.T., Adams, P.D., Clore, G.M., DeLano, W.L., Gros, P., Grosse-Kunstleve, R.W., Jiang, J.S., Kuszewski, J., Nilges, M., Pannu, N.S., et al. (1998). Crystallography & NMR system: a new software suite for macromolecular structure determination. Acta Crystallogr. D Biol. Crystallogr. *54*, 905–921.

CCP4 (Collaborative Computational Project, Number 4) (1994). The CCP4 suite: programs for protein crystallography. Acta Crystallogr. D Biol. Crystallogr. *50*, 760–763.

Cohen, S.X., Morris, R.J., Fernandez, F.J., Ben Jelloul, M., Kakaris, M., Parthasarathy, V., Lamzin, V.S., Kleywegt, G.J., and Perrakis, A. (2004). Towards complete validated models in the next generation of ARP/wARP. Acta Crystallogr. D Biol. Crystallogr. *60*, 2222–2229.

Cohen, M.S., Zhang, C., Shokat, K.M., and Taunton, J. (2005). Structural bioinformatics-based design of selective, irreversible kinase inhibitors. Science *308*, 1318–1321.

Fabian, M.A., Biggs, W.H., Treiber, D.K., Atteridge, C.E., Azimioara, M.D., Benedetti, M.G., Carter, T.A., Ciceri, P., Edeen, P.T., Floyd, M., et al. (2005). A small molecule-kinase interaction map for clinical kinase inhibitors. Nat. Biotechnol. *23*, 329–336.

Fukunaga, R., and Hunter, T. (1997). MNK1, a new MAP kinase-activated protein kinase, isolated by a novel expression screening method for identifying protein kinase substrates. EMBO J. *16*, 1921–1933.

Hanks, S.K., and Quinn, A.M. (1991). Protein kinase catalytic domain sequence database: identification of conserved features of primary structure and classification of family members. Methods Enzymol. *200*, 38–62.

Hubbard, S.R., Wei, L., Ellis, L., and Hendrickson, W.A. (1994). Crystal structure of the tyrosine kinase domain of the human insulin receptor. Nature *372*, 746–754.

Jauch, R., Bourenkov, G.P., Chung, H.R., Urlaub, H., Reidt, U., Jackle, H., and Wahl, M.C. (2003). The zinc finger-associated domain of the *Drosophila* transcription factor grauzone is a novel zinc-coordinating protein-protein interaction module. Structure *11*, 1393–1402.

Johnson, L.N., Noble, M.E., and Owen, D.J. (1996). Active and inactive protein kinases: structural basis for regulation. Cell *85*, 149–158.

Knauf, U., Tschopp, C., and Gram, H. (2001). Negative regulation of protein translation by mitogen-activated protein kinase-interacting kinases 1 and 2. Mol. Cell. Biol. *21*, 5500–5511.

Knighton, D.R., Zheng, J.H., Ten Eyck, L.F., Ashford, V.A., Xuong, N.H., Taylor, S.S., and Sowadski, J.M. (1991a). Crystal structure of the catalytic subunit of cyclic adenosine monophosphate-dependent protein kinase. Science *253*, 407–414.

Knighton, D.R., Zheng, J.H., Ten Eyck, L.F., Xuong, N.H., Taylor, S.S., and Sowadski, J.M. (1991b). Structure of a peptide inhibitor bound to the catalytic subunit of cyclic adenosine monophosphate-dependent protein kinase. Science *253*, 414–420.

Krishna, S.S., Majumdar, I., and Grishin, N.V. (2003). Structural classification of zinc fingers: survey and summary. Nucleic Acids Res. *31*, 532–550.

Manning, G., Whyte, D.B., Martinez, R., Hunter, T., and Sudarsanam, S. (2002). The protein kinase complement of the human genome. Science *298*, 1912–1934.

McRee, D.E. (1999). XtalView/Xfit–a versatile program for manipulating atomic coordinates and electron density. J. Struct. Biol. *125*, 156–165.

Mol, C.D., Fabbro, D., and Hosfield, D.J. (2004). Structural insights into the conformational selectivity of STI-571 and related kinase inhibitors. Curr. Opin. Drug Discov. Devel. *7*, 639–648.

Nagar, B., Bornmann, W.G., Pellicena, P., Schindler, T., Veach, D.R., Miller, W.T., Clarkson, B., and Kuriyan, J. (2002). Crystal structures of the kinase domain of c-Abl in complex with the small molecule inhibitors PD173955 and imatinib (STI-571). Cancer Res. *62*, 4236–4243.

Nikolcheva, T., Pyronnet, S., Chou, S.Y., Sonenberg, N., Song, A., Clayberger, C., and Krensky, A.M. (2002). A translational rheostat for RFLAT-1 regulates RANTES expression in T lymphocytes. J. Clin. Invest. *110*, 119–126.

Nolen, B., Taylor, S., and Ghosh, G. (2004). Regulation of protein kinases; controlling activity through activation segment conformation. Mol. Cell *15*, 661–675.

O'Loghlen, A., Gonzalez, V.M., Pineiro, D., Perez-Morgado, M.I., Salinas, M., and Martin, M.E. (2004). Identification and molecular characterization of Mnk1b, a splice variant of human MAP kinase-interacting kinase Mnk1. Exp. Cell Res. *299*, 343–355.

Otwinowski, Z., and Minor, W. (1997). Processing of X-ray diffraction data collected in oscillation mode. Methods Enzymol. *276*, 307–326.

Pargellis, C., Tong, L., Churchill, L., Cirillo, P.F., Gilmore, T., Graham, A.G., Grob, P.M., Hickey, E.R., Moss, N., Pav, S., and Regan, J. (2002). Inhibition of p38 MAP kinase by utilizing a novel allosteric binding site. Nat. Struct. Biol. *9*, 268–272.

Pyronnet, S., Imataka, H., Gingras, A.C., Fukunaga, R., Hunter, T., and Sonenberg, N. (1999). Human eukaryotic translation initiation factor 4G (eIF4G) recruits mnk1 to phosphorylate eIF4E. EMBO J. *18*, 270–279.

Reiling, J.H., Doepfner, K.T., Hafen, E., and Stocker, H. (2005). Diet-dependent effects of the *Drosophila* Mnk1/Mnk2 homolog Lk6 on growth via eIF4E. Curr. Biol. *15*, 24–30.

Richter, J.D., and Sonenberg, N. (2005). Regulation of cap-dependent translation by eIF4E inhibitory proteins. Nature *433*, 477–480.

Scheper, G.C., Morrice, N.A., Kleijn, M., and Proud, C.G. (2001). The mitogen-activated protein kinase signal-integrating kinase Mnk2 is a eukaryotic initiation factor 4E kinase with high levels of basal activity in mammalian cells. Mol. Cell. Biol. *21*, 743–754.

Scheper, G.C., Parra, J.L., Wilson, M., Van Kollenburg, B., Vertegaal, A.C., Han, Z.G., and Proud, C.G. (2003). The N and C termini of the splice variants of the human mitogen-activated protein kinase-interacting kinase Mnk2 determine activity and localization. Mol. Cell. Biol. *23*, 5692–5705.

Seethala, R., and Menzel, R. (1998). A fluorescence polarization competition immunoassay for tyrosine kinases. Anal. Biochem. *255*, 257–262.

Slentz-Kesler, K., Moore, J.T., Lombard, M., Zhang, J., Hollingsworth, R., and Weiner, M.P. (2000). Identification of the human Mnk2 gene (MKNK2) through protein interaction with estrogen receptor β. Genomics *69*, 63–71.

Taylor, S.S., and Radzio-Andzelm, E. (1994). Three protein kinase structures define a common motif. Structure *2*, 345–355.

Tereshko, V., Teplova, M., Brunzelle, J., Watterson, D.M., and Egli, M. (2001). Crystal structures of the catalytic domain of human protein kinase associated with apoptosis and tumor suppression. Nat. Struct. Biol. *8*, 899–907.

Ueda, T., Watanabe-Fukunaga, R., Fukuyama, H., Nagata, S., and Fukunaga, R. (2004). Mnk2 and Mnk1 are essential for constitutive and inducible phosphorylation of eukaryotic initiation factor 4E but not for cell growth or development. Mol. Cell. Biol. *24*, 6539–6549.

von der Haar, T., Gross, J.D., Wagner, G., and McCarthy, J.E. (2004). The mRNA cap-binding protein eIF4E in post-transcriptional gene expression. Nat. Struct. Mol. Biol. *11*, 503–511.

Waskiewicz, A.J., Flynn, A., Proud, C.G., and Cooper, J.A. (1997). Mitogen-activated protein kinases activate the serine/threonine kinases Mnk1 and Mnk2. EMBO J. *16*, 1909–1920.

Waskiewicz, A.J., Johnson, J.C., Penn, B., Mahalingam, M., Kimball, S.R., and Cooper, J.A. (1999). Phosphorylation of the cap-binding protein eukaryotic translation initiation factor 4E by protein kinase Mnk1 in vivo. Mol. Cell. Biol. *19*, 1871–1880.

Wilson, K.P., Fitzgibbon, M.J., Caron, P.R., Griffith, J.P., Chen, W., McCaffrey, P.G., Chambers, S.P., and Su, M.S. (1996). Crystal structure of p38 mitogen-activated protein kinase. J. Biol. Chem. *271*, 27696–27700.

Accession Numbers

Coordinates and structure factors have been submitted to the RSCB Protein Databank (http://www.rcsb.org/pdb/) with accession codes 2AC3 and 2AC5 and will be released upon publication.